THE JOURNAL OF PHYSICAL CHEMISTRY LETTERS
A JOURNAL OF THE AMERICAN CHEMICAL SOCIETY

pubs.acs.org/JPCL

Letter

Configurational Entropy Effects on Glass Transition in Metallic Glasses

Ming Yang, Wenyue Li, Xiongjun Liu,* Hui Wang, Yuan Wu, Xianzhen Wang, Fei Zhang, Qiaoshi Zeng, Dong Ma, Haihui Ruan,* and Zhaoping Lu*

Cite This: *J. Phys. Chem. Lett.* 2022, 13, 7889−7897

Read Online

HPSTAR 1565-2022

ACCESS | Metrics & More | Article Recommendations | Supporting Information

ABSTRACT: Configurational entropy (S_{conf}) is known to be a key thermodynamic factor governing a glass transition process. However, this significance remains speculative because S_{conf} is not directly measurable. In this work, we demonstrate the role of S_{conf} theoretically and experimentally by a comparative study of a Zr−Ti−Cu−Ni−Be high-entropy metallic glass (HE-MG) with one of its conventional MG counterparts. It is revealed that the higher S_{conf} leads to a glass that is energetically more stable and structurally more ordered. This is manifested by *ab initio* molecular dynamics simulations, showing that ∼60% fewer atoms are agitated above T_g, and experimental results of smaller heat capacity jump, inconspicuous stiffness loss, insignificant structural change during glass transition, and a more depressed boson peak in the HE-MG than its counterpart. We accordingly propose a model to explain that a higher S_{conf} promotes a faster degeneracy-dependent kinetics for exploration of the potential energy landscape upon glass transition.

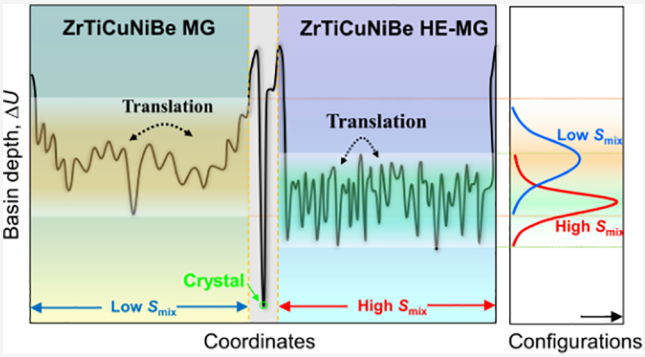

If a liquid is cooled fast enough to depress crystallization, the liquid structure can be vitrified at a glass transition temperature, T_g,[1] with the viscosity of the supercooled liquid (SCL) increasing dramatically to a reference magnitude (usually 10^{12} Pa·s). The resultant glass possesses all the salient microscopic features of a liquid except that it does not flow. Such a phenomenological definition of glass transition (GT) brings up an open question in condensed matter physics, namely, how atoms slow down and become constrained in a narrow temperature regime near T_g.[2] Gibbs and Dimarzio[3] formulated a classic description of GT in which a glass below T_g is frozen in a single configuration, while the equilibrium liquid above T_g is free to explore all possible configurations. This formulation lays a robust foundation for the Adam−Gibbs relation,[4,5] which provides a connection between dynamics and configurations of a glass; that is, relaxation time is a function of configurational entropy. The classic Gibbs−Dimarzio description also inspired an entropic description of glass relaxation and GT based on the concept of the potential energy landscape (PEL), which was originally proposed by Goldstein[6] and later employed in many studies.[2,7] The minima of PEL are referred to inherent structures (ISs), and the entropy of a glassy material is dependent on both IS and temperature. The precipitous increase in viscosity and decrease in heat capacity during cooling is due to the constraint in exploring IS based on the Arrhenius kinetics of barrier crossing. To validate this entropic picture, the configurational and vibrational contributions to an excess entropy during glass transition have been separately evaluated for molecular and network glasses,[8,9] Lennard-Jones liquids,[10,11] as well as metallic glasses (MGs).[12] In the SCL of MGs, Smith *et al.*[12] suggested that the vibrational entropy is trivial in comparison to its configurational counterpart, and the excess entropy of MGs is almost entirely configurational, which is consistent with the conception of Gibbs and Dimarzio.[3] Through molecular dynamics (MD) simulations, Han *et al.*[13] recently revealed that the hidden structural mechanism underlying a configurational entropic kink at glass transition is the proliferation of a high degree of centrosymmetric (rigid) structures.

Although these investigations confirm the entropic picture in understanding GT and the associated critical phenomena, it is still unclear how to modify the entropy of an amorphous system and study its effect on the GT-associated critical phenomena. Recently, developing new materials by employing the concept of mixing entropy (S_{mix}) has been emerging as a hot topic in materials science. Maximizing the S_{mix} in crystalline materials leads to the family of high-entropy alloys (HEAs).[14] It was argued that the maximum S_{mix} stabilizes the

Received: April 25, 2022
Accepted: August 10, 2022
Published: August 18, 2022

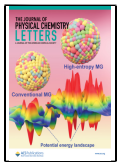

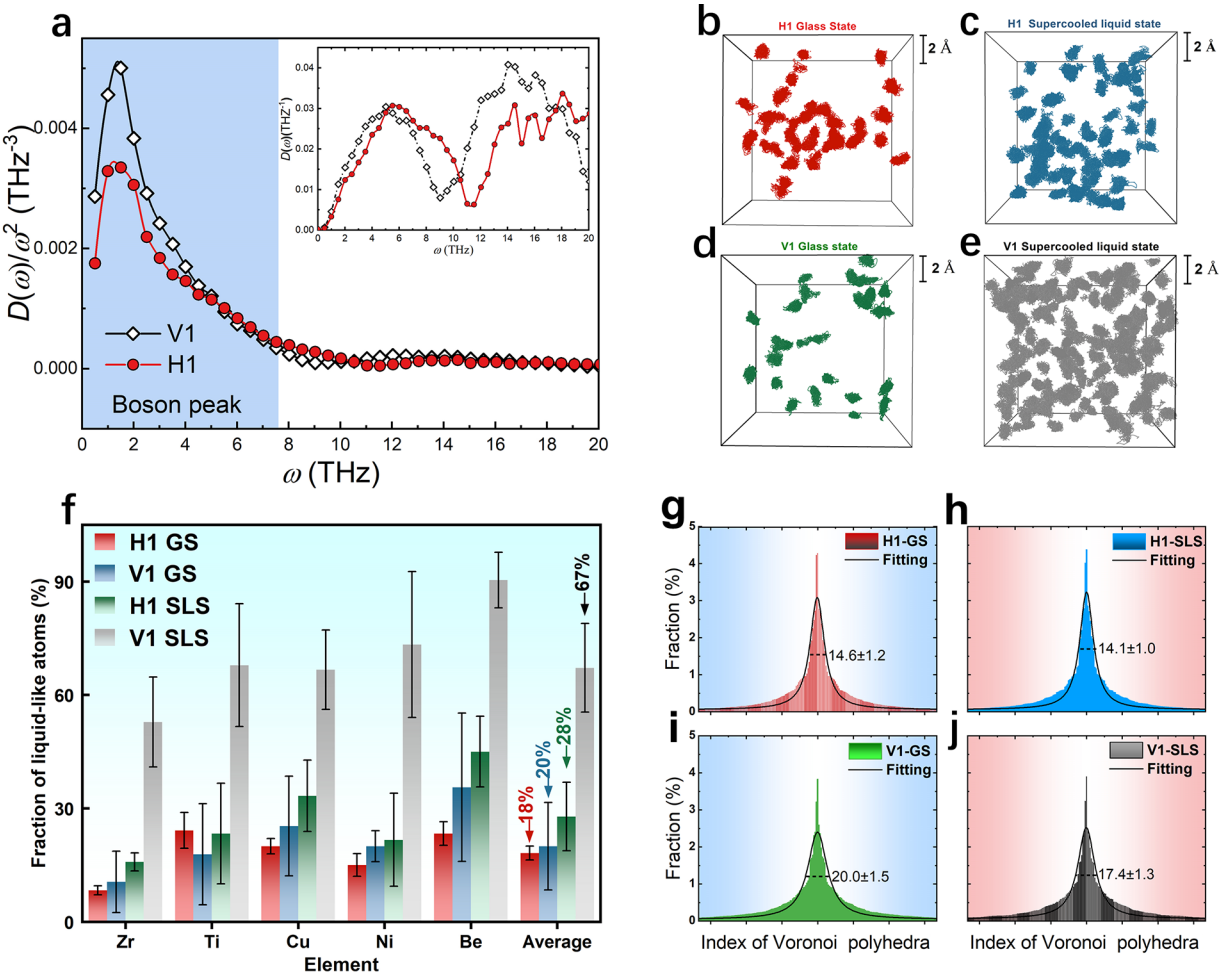

Figure 1. *Ab initio* molecular dynamics (AIMD) simulated data. (a) The reduced vibrational density of states (VDOS) $D(\omega)/\omega^2$ simulated at 300 K for H1 and V1. Inset: VDOS $D(\omega)$. (b–e) The movement trajectory of liquid-like atoms (LLAs) from the glass state to supercooled liquid state for H1 and V1. (f) Quantification of LLAs at a given moment of the glass state (GS) and supercooled liquid state (SLS) for V1 (blue and gray) are 20% and 67%, and for H1 (red and green) are 18% and 28%, respectively. (g–j) Distribution of Voronoi polyhedra of V1 and H1 from the glass state to supercooled liquid state. The peak center at the middle represents the Voronoi polyhedron ⟨0, 4, 4, 2⟩.

melts (avoiding phase separation in cooling)[15] and renders simple solid solutions with attractive properties.[16−18] Analogous to HEAs, the equiatomic multicomponent alloys with an amorphous structure are termed as high-entropy metallic glasses (HE-MGs). In terms of atomic structure, HE-MGs exhibit similar structural features compared with conventional glassy solids, i.e., mazelike selected area electron diffraction pattern and broad diffraction maxima characteristics in X-ray diffraction data.[19,20] However, HE-MGs exhibit some unique properties, such as large magnetocaloric effect,[21] tunable catalytic performance,[22] and improved mechanical properties and corrosion resistance.[23] In particular, our previous studies revealed that HE-MGs have sluggish crystallization kinetics,[24,25] which was related to slow diffusion, a conceptualized effect induced by high S_{mix}.

The emergence of HE-MGs has filled in a missing part in the "jigsaw" of the entropic picture, as one is able to tweak the configurational entropy by simply adjusting the alloy composition. Most importantly, this is easily doable in experiments. Thus, questions naturally arise regarding how an amorphous system with a well-defined increase in S_{conf} is changed in terms of GT phenomena, structure, and dynamics. In an effort to answer these questions, we have conducted *ab initio* molecular dynamics (AIMD) simulations and experiments to comparatively investigate the glassy structure and GT-associated phenomena of a conventional MG and its HE counterpart. Our results reveal that a higher S_{conf} leads to a glass that is energetically more stable and structurally more ordered. Computationally, the higher stability and homogeneity are evidenced by the smaller change in average atomic mobility (or less structural changes) during GT and the suppressed boson peak in the vibrational density of states (VDOS), respectively. Experimentally, they are supported by the cryogenic and near-T_g calorimetry measurements, *in situ* Young's modulus measurements, and synchrotron X-ray characterizations. Moreover, it was revealed that the HE-MG exhibits a higher degree of structural order than the conventional MG does, consistent with the existing findings[26] and explaining the higher structural stability and homogeneity. Considering these results, we proposed a simplified kinetic picture of GT to understand the effects of S_{mix} in glass; that is, the increase in S_{conf} due to higher S_{mix} corresponds to a faster degeneracy-dependent PEL exploration kinetics.

The prototypical HE-MG $Zr_{20}Ti_{20}Cu_{20}Ni_{20}Be_{20}$ (H1) and its conventional MG counterpart Vitreloy 1 with the composition of $Zr_{41.2}Ti_{13.8}Cu_{12.5}Ni_{10}Be_{22.5}$ (V1) were com-

https://doi.org/10.1021/acs.jpclett.2c01234
J. Phys. Chem. Lett. 2022, 13, 7889−7897

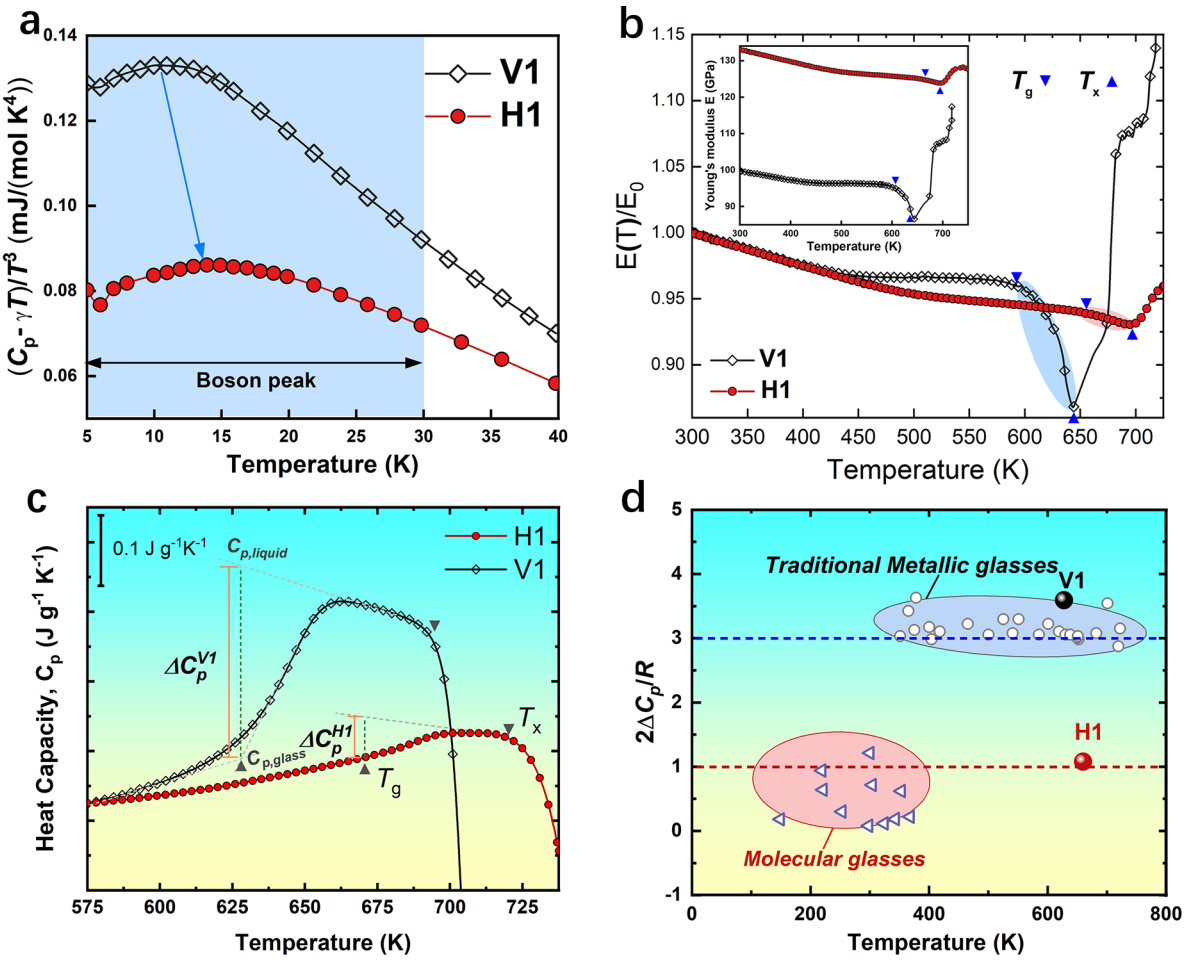

Figure 2. Experimental data for H1 and V1. (a) Low-temperature specific heat capacity for H1 and V1. The arrow indicates the lower boson peak intensity of H1 in comparison to that of V1. It is seen that the experimental boson peak intensity shows the same trend as the simulated data. (b) Diagram of normalized *in situ* Young's modulus as a function of temperature for H1 and V1. E_0 is Young's modulus at room temperature. The inset is the temperature dependence of the actual Young's modulus of H1 and V1, and the higher Young's modulus at room temperature of H1 indicates the stiffer atomic bonding or higher compactness in the HE-MG. (c) Specific heat capacity, C_p, and the jump of heat capacity, ΔC_p^{H1} and ΔC_p^{V1}, during GT, respectively, for H1 and V1, as illustrated by the dashed lines. (d) Correlation of the reduced heat capacity jump, $2\Delta C_p/R$ (R, the gas constant), with the glass transition temperature, T_g, in our HE-MGs, as compared with a variety of glasses.[45−52]

pared (note that the constitutional elements of H1 are identical to those of V1). The AIMD simulations were performed to investigate the atomic dynamics of H1 and V1 (for more details, see the Supporting Information). Figure 1a displays the reduced vibrational density of states (VDOS) of H1 and V1, and the corresponding VDOS $D(\omega)$ is in the inset. The VDOS $D(\omega)$ of the glass was calculated by taking the Fourier transformation of the computed velocity autocorrelation functions (VACFs)[27] at 300 K (Supporting Information). For glasses lacking long-range order, their VDOS usually display an excess peak over the Debye square-frequency law at low frequencies, leading to the boson peak (BP),[28,29] which manifests the intrinsic structural heterogeneity of a glass (known as the "fingerprint" of a glass).[29−31] The BP can be characterized in terms of the BP frequency ω_{BP} and the intensity I_{BP}, defined as $I_{BP} = D(\omega_{BP})/\omega_{BP}^2$ where $D(.)$ is the VDOS function. Note that the BP intensities in these two samples are significantly different. The BP intensity of H1 is much more depressed than that of V1, implying that the inherent structure in H1 is more homogeneous. Conceptually, a spatially heterogeneous system can be regarded as a distribution of IS with various compactness or potential energy. Those with high potential energies are considered to be liquid-like regions.[32] It is found that the increase in their volume fraction, through the methods such as hyperquenching,[33] addition of foreign atoms,[34] or plastic deformation,[31] leads to the more heterogeneous structure and the higher BP. Along this line, the depressed BP in the HE-BMG indicates the smaller or rarer liquid-like regions, and more likely, it is the increase in S_{conf} that makes H1 more homogeneous with less liquid-like regions.

With the structural information on H1 as implied by the depressed BP, we move on to unveil how it influences atomic mobility in GT. In AIMD simulations we quantified liquid-like atoms (LLAs) at temperatures between $T_g - 50$ K and $T_g + 50$ K to represent the glass state and supercooled liquid state for both MGs. The simulated T_g for H1 and V1 is estimated to be 950 and 850 K, respectively, which was determined by the temperature when the splitting of the second peak in pair distribution function curves occurred. The Debye−Waller factor (DWF), defined as the mean squared deviation of an atom from its equilibrium position,[35] was employed to differentiate LLAs from solid-like atoms (SLAs). Specifically, according to the Lindeman criterion,[36,37] the atoms with DWF

https://doi.org/10.1021/acs.jpclett.2c01234
J. Phys. Chem. Lett. 2022, 13, 7889−7897

larger than $(0.1 \times a)^2$ are identified as LLAs and others as SLAs, where a is the average bond length defined at the first minimum in the pair distribution function $g(r)$ for each type of element, as marked by the arrows in Figure S2, and the detailed data of $(0.1 \times a)^2$ for each element are listed in Table S1. Our computational models have 200 atoms, and their DWFs are shown in Figure S3, where the critical magnitude of $(0.1 \times a)^2$ is indicated for each type of atom. Comparing the atomic models at $T_g - 50$ K and $T_g + 50$ K, it is observed that the increase in the number of LLAs in H1 is much smaller than that in V1 when the system underwent a GT event.

We further scrutinized the trajectories of LLAs in the glassy and supercooled liquid states and present the results in Figure 1b−e. In the glassy state, both H1 and V1 possess a very small number of LLAs, with the quantity in V1 slightly higher than that in H1, as shown in Figure 1b,d. When the systems were heated into their supercooled liquid regions, many more atoms in V1 (Figure 1e) become LLAs than those in H1 (Figure 1c). The comparison of panels c and e in Figure 1 brings about the impression that the regions experiencing the SLA-to-LLA transition are overwhelming in V1 but indistinct in H1. Figure 1f compares the percentage of LLAs at a moment during relaxation in the supercooled liquid states of H1 and V1. The average contents of LLAs are 28% and 67% for H1 and V1, respectively; that is, the increase in S_{conf} by maximizing S_{mix} causes ∼60% fewer atoms being agitated during GT. According to the percolation theory,[38−40] there is a percolation threshold p_c (basically a constant ∼15%) for a perfectly random three-dimensional system with spherical particles, above which unbounded clusters of connected sites occur. In H1, the LLA fraction of 28% in the supercooled liquid state is above this theoretical threshold p_c; therefore, it is expected that the macroscopic GT behavior of H1 can still be observed (e.g., low viscosity can be measured[24,25]). Furthermore, fewer LLAs involved in the GT of H1, as shown in Figure 1c, means a large quantity of atoms remains constrained and stays relatively intact as the solid-like skeletons; therefore, it is inferred (and verified by experiments) that the loss of the stiffness of H1 is insignificant during GT. Note that the values of the average content of LLAs at $T_g - 50$ K for both H1 (18%) and V1 (20%) are still higher than the percolation threshold p_c because the ultrahigh cooling rate of 5×10^{12} K/s in AIMD renders relatively loosely packed glasses at $T_g - 50$ K, leaving a certain level of atomic mobility. However, the contents of LLAs in H1 and V1 at $T_g - 50$ K have become very close to each other, indicating the trend of vitrification.

To obtain more detailed structural information, Voronoi tessellation analysis was conducted for all AIMD models at $T_g \pm 50$ K after structural relaxation. Figure 1g−j displays the statistical distribution of the occurrence of all polyhedrons (∼1000 types) and implies that the polyhedral fractions exhibited a bell-shaped distribution, which can be fitted by the Voigt function to quantify the full width at half-maximum (fwhm) of the distribution. It is found that the change of fwhm during GT (i.e., from $T_g - 50$ K to $T_g + 50$ K) is insignificant for H1, decreasing by only 3.4% from the glassy state (fwhm = 14.6 ± 1.2) to the supercooled liquid state (fwhm = 14.1 ± 1.0). In contrast, the change in fwhm for V1 is remarkable (from 20.0 ± 1.5 to 17.4 ± 1.3, i.e., 13% reduction). The implication is, again, the structural rearrangement in H1 is very insignificant, consistent with the above LLA results. The details of the 30 most frequent Voronoi polyhedra are shown in Figure S4, indicating that H1 and V1MGs have similar polyhedral structures in glassy and SCL states.

The structural analysis exhibited in Figure 1g−j contains further details worth emphasizing. First, the distribution of Voronoi polyhedron in the glass state of H1 is narrower than that in V1 in terms of the sorted histogram as shown in Figure 1g,i. Though this difference is subtle in AIMD simulations because of the limits of the length and time scales, it implies that the structures in H1 are more homogeneous, consistent with the BP result as shown in Figure 1a. Also, the higher content of polyhedron (Voronoi index: ⟨ 0, 4, 4, 2⟩ and ⟨0, 4, 4, 0⟩) and smaller fwhm spanning the Voronoi polyhedron peak in H1 than those in V1 imply the higher degree of structural order in H1. All these implications will be evidenced by the following experimental results.

Experimentally, the BP depression due to the higher S_{conf}, as exhibited by $D(\omega)/\omega^2$ in Figure 1a, can also be determined by the temperature dependence of heat capacity (C_p) at low temperatures.[28,32,41] Figure 2a exhibits the measured heat capacity results in the form of $(C_p - \gamma T)/T^3$ versus T. Note that the electronic heat capacity has no contribution to a BP, but it would become considerable at low temperatures. Thus, the electronic heat capacity needs to be determined and subtracted from the measured total heat capacity of the glasses to highlight the BP contribution. Therefore, we fitted the C_p data in the cryogenic regime ($T \leq 8$ K) with the equation $C_p/T = \beta T^2 + \gamma$ following refs 42 and 43, where γ and β are the coefficients signifying the electronic and phonon contributions, respectively. The values of γ and β are 3.46 mJ/mol K^2 and 130.3 μJ/mol K^4 for V1 and 3.06 mJ/mol K^2 and 80.7 μJ/mol K^4 for H1, respectively. Similar to the simulated BP data (Figure 1a), experimental measurements of low-temperature specific heat capacity also indicate that the BP intensity of H1 is much more depressed as compared with that of V1, indicating the higher structural homogeneity in H1.

We then measured the temperature dependence of Young's modulus (E) of the as-cast H1 and V1 from 300 to 750 K, the temperature ranges below the crystallization temperature T_x (Figure 2b). The corresponding temperature dependence of Young's modulus (E) is shown in the inset of Figure 2b. The Young's modulus of H1 is always higher than that of V1, indicating the stiffer atomic bonding or higher compactness in the HE-MG. For better illustration, the change in Young's modulus as a function of temperature T was normalized by that obtained at room temperature, E_0, and the curves are replotted in Figure 2b. When $T < T_g$, all the $E-T$ curves exhibit two stages: in the first stage, below 450 K for V1 and below 500 K for the HE-BMGs, the Young's modulus decreases linearly with temperature because of the effect of thermal expansion; in the second stage, the decreasing rate reduces, caused by the sub-T_g local atomic rearrangements.[44] When $T > T_g$, the Young's modulus of V1 reduces much more precipitously than that of H1. When $T > T_x$, the sudden increase of Young's modulus above T_x is caused by crystallization. For another HE-MG ZrTiCuNiHf (H2), we also obtained similar results of Young's modulus variation (Figure S5); that is, the reduction of Young's modulus in an HE-MG is inconspicuous during GT, indicating the limited structural relaxation, consistent with the mobility and structural analyses by AIMD simulations.

Figure 2c shows the temperature dependence of C_p during GT. In the calorimetry studies with MGs, it is found that the change of specific heat during GT, denoted by ΔC_p, is a nearly

https://doi.org/10.1021/acs.jpclett.2c01234
J. Phys. Chem. Lett. 2022, 13, 7889−7897

constant $3k_B/2$.[45] This was interpreted to be the result of the unconstrained three translational degrees of freedom (DOFs) for each of the atoms based on the model of simple liquids.[46] During heating, the C_p of glass increases; after a maximum, the C_p of supercooled liquid decreases. ΔC_p is then defined as the difference of glass and supercooled liquid C_p at T_g when they are extrapolated to T_g.[45] The T_g for H1 and V1, based on calorimetry studies, are 669 and 629 K, respectively, which is lower than the simulated T_g because the cooling rate in AIMD ($\sim 5 \times 10^{12}$ K/s) is much faster than that of experiments ($\sim 4 \times 10^4$ K/s). We found that the ΔC_p of V1 and H1 are approximately $3k_B/2$ and $k_B/2$, respectively, as shown in Figure 2c. A similar ΔC_p value of $k_B/2$ was also observed for another HE-MG (H2), as shown in Figure S6. We include the ΔC_p data of various MGs and molecular glasses in Figure 2d. These data clearly demonstrate that the often-assumed invariance of $\Delta C_p \approx 3k_B/2$ for conventional MGs[45] has been severely violated by the HE-MGs. Instead, ΔC_p of HE-MGs is similar to molecular glasses in which atoms are more constrained by the covalent bonding.[45−52] According to the model of simple liquids,[46] the result of ΔC_p (T_g) $\approx k_B/2$ for HE-MGs signifies that the translational DOF is significantly constrained when an HE-MG transforms into the supercooled liquid. This anomalously low ΔC_p is consistent with the previous argument on the lower atomic mobility in H1 during GT as inferred from Figure 1; that is, the small number of LLAs gives rise to the small average DOF per atom and the low ΔC_p.

Further structural analyses have been performed by comparing the real-space pair distribution functions (PDFs), $G(r)$, of H1 and V1 at their glass and supercooled liquid states (Figure 3). The PDF data were collected by synchrotron X-ray diffraction (see details in the Supporting Information). For H1, the peak position of each shell shifts to the lower correlation length at both the glass and supercooled liquid states in comparison to those of V1, as shown in Figure 3a. By calculating the atomic number density $\rho_0 = \frac{N_A}{M}\rho_m$, where M is the molar mass, N_A the Avogadro constant, and ρ_m the sample mass density (the densities of H1 and V1 are 6.602 and 6.383 g/cm^3, respectively), we found that H1 has 16% higher number density ($\sim$0.074 Å^{-3}) than V1 ($\sim$0.064 Å^{-3}). In addition, Figure 3a shows that the $G(r)$ of H1 can oscillate to the 10th shell, much further than that of V1 in which the 7th shell cannot be discerned. This result indicates the more ordered or far-reaching medium range ordered structure in H1. Figure 3b shows the differences in $G(r)$ between the glass and supercooled liquid states, $\Delta G(r) = G(r)_{Tg-20K} - G(r)_{Tx-20K}$. It is noted that $\Delta G(r)$ fluctuates much more significantly in V1 than in H1, particularly in the range from 2.5 to 7.5 Å, indicating that the structural change during GT is more insignificant in H1. These structural data further support the above agreements based on the AIMD simulations and the measured temperature dependences of C_p and E; that is, the higher S_{mix} promotes a more ordered and stable atomic packing structure.

In this work, we follow the concept of HEAs to understand the effect of high S_{mix} on formation of an HE-MG.[14] It is conceivable that the melt of a multicomponent system can be regarded as an ideal mixing model. Hence, it is undoubtful that the H1 melt has a larger S_{conf} than the V1 melt. In what follows, we propose a simplified kinetics model to reconcile and make clear these observations based on the concept of PEL. Consider that a macroscopic system can be represented by

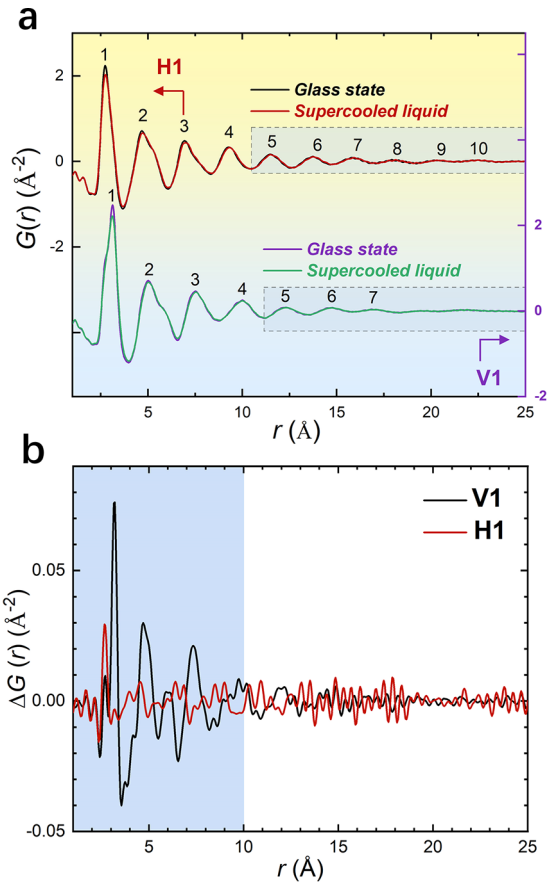

Figure 3. Structural analysis in real space of H1 and V1. (a) Pair distribution function (PDF) $G(r)$ curves for H1 and V1 at the glass and supercooled liquid state. (b) The $G(r)$ difference $\Delta G(r) = G(r)_{Tg-20K} - G(r)_{Tx-20K}$ between glass and supercooled liquid states.

an atomic subsystem of N atoms with M types of elements. For glass transition, it was argued that the typical size of such a subsystem is $N \approx 10^2$.[53] The PEL of such a subsystem contains many basins (i.e., IS) with the basin depth ΔU (negative value), which is the difference between the minimum of the basin and the energy of its ergodicity state. The entropy associated with ΔU_k and with a given configuration C_i may be expressed as[54]

$$S_C(C_i, \Delta U_k) = S_P(P|(C_i, \Delta U_k)) + \sum_j q_j S_V(\Phi|(P_j, C_i, \Delta U_k)) \quad (1)$$

where S_P is the entropy arising from the permutations of atoms; the argument $P|(C_i, \Delta U_k)$ represents all possible stable permutations based on the configuration C_i to render the basin depth ΔU_k; q_j is the possibility of taking the permutation P_j; S_V is the vibrational entropy, and the argument $\Phi|(P_j, C_i, \Delta U_k)$ represents all vibration modes when the permutation, configuration, and potential energy minimum are fixed. Traditionally, the permutation entropy S_P is ignored in metallic systems because an alloy design is generally a microalloying process; the tiny change in composition does not lead to a significant change in S_P. With the advent of high-entropy metallic system, S_P becomes no longer negligible. Consider an ideal scenario that all permutations are possible (i.e., the induced change in ΔU is negligible), the number of

https://doi.org/10.1021/acs.jpclett.2c01234
J. Phys. Chem. Lett. 2022, 13, 7889−7897

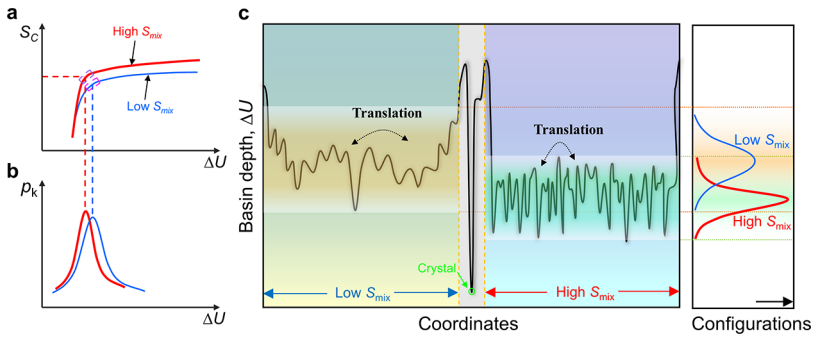

Figure 4. Understanding the effect of S_{mix} on different glass-forming liquids from the PEL perspective. (a) A schematic description of the relation between configurational entropy S_C and basin depth ΔU for different metallic glassy systems. (b) The probility distribution of subsystem configuration with respect to ΔU upon cooling. (c) Schematic representation of the basin depth ΔU for metallic glasses with high and low S_{mix}. For the system with high S_{mix}, the atomic configurations exhibited more ergodicity with a wider energy drop (ΔU) from the melt. In the system with low S_{mix}, the energy drop (ΔU) is small. ΔU is a negative value.

permutations is $\Omega_P = N!/\prod_{i=1}^{M}(c_iN)!$. Using Stirling's approximation, the Boltzmann entropy of permutation is

$$S_P = k_B \ln \Omega_P = k_B\left(-N\sum_{i=1}^{M} c_i \ln c_i - M + 1\right) \approx NS_{mix} \tag{2}$$

Therefore, in the ideal case, the permutation entropy is exactly the product of N and S_{mix}. We then move on to see how the mixing entropy enters the configuration entropy. Discarding the vibrational one, the configurational entropy associated with a basin k is given by[55,56]

$$S_C(\Delta U_k) = -k_B\sum_i q_{ik}\ln q_{ik} + \sum_i q_{ik}S_P(P|(C_i, \Delta U_k)) \tag{3}$$

where q_{ik} is the probability of observing a configuration C_i with the basin k, and the first term on the right-hand side is the Gibbs entropy associated with the distribution q_{ik}. If $S_P \approx NS_{mix}$, eq 3 becomes

$$S_C(\Delta U_k) \approx -k_B\sum_i q_{ik}\ln q_{ik} + NS_{mix} \tag{4}$$

The total configurational entropy is then

$$S_{conf} = -k_B\sum_k p_k \ln p_k + \sum_k p_k S_C(\Delta U_k) \tag{5}$$

where p_k is the probability of occupying the basin k. If the system is in equilibrium (or detail-balanced), p_k assumes a Boltzmann distribution: $p_k^e \propto \exp\left(-\frac{\Delta U_k - TS_C(\Delta U_k)}{k_BT}\right)$ (the superscript e represents equilibrium). For an ideal case, substituting eq 4 into eq 5 leads to

$$S_{conf} = -k_B\sum_k p_k \ln p_k - k_B\sum_k p_k\sum_i q_{ik}\ln q_{ik} + NS_{mix} \tag{6}$$

Equation 6 is the illustration of how the mixing entropy contributes to the configurational entropy. For nonideal cases, eq 2 no longer holds, but it is still justifiable that the HE-MG has a higher S_{conf} than MG owing to the larger S_{mix}, which, after multiplying by N, is indispensable.

Still lingering is how the higher S_{mix} leads to the more stable glass based on the above comparison between H1 and V1. To answer this question, we shall employ a simplified model of structural relaxation that involves entropy-dependent kinetics. Let us first assume that structural relaxation at a temperature is to let the distribution p_k approach the Boltzmann distribution p_k^e. For such a process, the simplest dynamics can be described by the following master equations (MEs):

$$\frac{dp_k}{dt} = -w_{kj}p_k + w_{jk}p_j \tag{7}$$

where w_{kj} (or w_{jk}) is the hopping rate from the potential energy minimum k to j (or j to k). The analytical solutions of ME eq 7 require further simplifications of the above system, for example, assuming only two or three basins (i.e., the two-level[57] or three-level models[58]) or infinitesimal deviation from an equilibrium state.[59] If the hopping between basins k and j needs to cross the same saddle-point energy $U_{kj} = U_{jk}$, the hopping rate is expressed as

$$w_{kj} = \nu_0\exp\left(-\frac{U_{kj} - \Delta U_k - TS_C(\Delta U_j)}{k_BT}\right) \tag{8}$$

where ν_0 is the attempting rate proportional to atomic vibration frequency. One can easily verify that the detail-balanced solution of eqs 7 and 8 is p_k^e. With such a model, a cooling process shifts the distribution p_k toward the low-energy side. Because the internal kinetics w_{kj} reduces exponentially with the reciprocal temperature $(1/T)$, at a critical $T \sim T_g$, the shift of p_k is stopped and the distribution of the subsystem configuration is frozen; that is, a glass transition occurs. This ME-based description of structural relaxation in glass has been employed to study various complicated relaxation phenomena (e.g., memory effect or Kovacs hump).[58,60,61] Herein, we also employ it to give a qualitative account on the effect of S_{mix}.

We assume that the configurational entropy S_C associated with a minimum U_k can be analytically expressed. As an example, for simple systems such as Lennard-Jones liquid,[62] silica,[63] or selenium,[64] it was shown that $S_C(\Delta U)$ was approximately a half Gaussian with a fast-decaying tail in a low-energy regime. For the MGs herein, as the relation $S_C(\Delta U)$ is unknown, we draw the schematics of $S_C(\Delta U)$ for H1 and V1 in Figure 4a following the above references. Owing to the difference in S_{mix} and based on eq 4, it is shown that the $S_C(\Delta U)$ of H1 is higher than that of V1, and the upper shift must be bounded by $N\Delta S_{mix}$. For V1 and H1 with $N = 10^2$ ($N \sim 10^2$ represents the typical size of such a subsystem[53]), $N\Delta S_{mix} = 14.5k_B$ (the difference in S_{mix} between V1 and H1 is

https://doi.org/10.1021/acs.jpclett.2c01234
J. Phys. Chem. Lett. 2022, 13, 7889−7897

approximately $0.145k_B$). With eq 8, it means that the hopping in the PEL of H1 is much faster than that in the PEL of V1; that is, for the same energy barrier, $1 \ll w_{kj}^{H1}/w_{kj}^{V1} \leq \exp(N\Delta S_{mix}/k_B) = 2 \times 10^6$. Note that both V1 and H1 alloys were obtained with the same cooling rate in experiment; the higher hopping rate (i.e., the lower viscosity for H1 melts have been measured than that of V1[24]) in H1 can allow the system to explore a larger energy regime than that of V1 before the amorphous system is frozen, as illustrated in Figure 4b. That is, the atomic subsystems in H1 can reach deeper basins during cooling. Also, the distribution p_k in H1 can be narrower because the faster kinetics regulated by w_{kj} push p_k into the region of the fast-decaying tail of $S_C(\Delta U)$ as indicated by the brackets in Figure 4a; this explains qualitatively the higher structural stability and more ordered structure in H1, *i.e.*, the HE-MG exhibits the suppressed boson peak intensity (Figures 1a and 2a) and larger atomic correlation length (Figure 3a). Figure 4c depicts schematically the energetic minimum landscape of the systems with crystalline phases. These results demonstrate the higher thermal stability (i.e., low atomic motion ability, as shown in Figure 1b,c), higher resistance to softening (Figure 2b), smaller translational DOFs (Figure 2c), and insignificant structural changes during GT (Figure 3b) in HE-MGs. The quenched H1 should be situated in a more stable and more ordered energy state than that of V1, but it can still have a large number of configurations because of the higher S_{mix} (Supporting Information, Table S2), corresponding to the greater number of permutations of atoms. Therefore, the S_{conf} in the more ordered HE-MG does not have to be low (Supporting Information, Figure S7).

In summary, with AIMD simulations as well as experimental observations, we have revealed that upon cooling, the higher S_{conf} can lead to the more stable and ordered glass. In the heating process, atoms in an HE-MG with a large S_{conf} in have low atomic motion ability and small translational DOFs, leading to the insignificant structural change, higher resistance to softening, and smaller latent heat jump during GT. With the master equations-based model of GT, we propose a qualitative explanation for all the observations: the increase in S_{conf} due to higher S_{mix} corresponds to a faster degeneracy-dependent kinetics for exploration of PEL. This S_{conf} effect results in a structurally more ordered and energetically more stable atomic packing, with extremely insignificant atomic structural changes during GT in HE-MGs, as compared with their conventional MG counterparts. In a nutshell, the entropy stabilizing effect is that with similar chemical compositions, the HE-MG exhibits larger energy drops from the melt and becomes more ordered than the conventional MG. Our findings provide important implications for understanding the nature of glass transition and developing novel glassy or disordered materials that are favored by high S_{conf}.

■ ASSOCIATED CONTENT

Supporting Information

The Supporting Information is available free of charge at https://pubs.acs.org/doi/10.1021/acs.jpclett.2c01234.

VACFs as a function of time; definition of the cutoff a in the $g(r)$ for each type of element; distributions of the 30 most frequent Voronoi polyhedra at different states; detailed definition of the DWF of the individual atoms; *in situ* Young's modulus data and the jump of heat capacity ΔC_p (T_g) during glass transition of HE-BMG and $Zr_{20}Ti_{20}Hf_{20}Cu_{20}Ni_{20}$; calculated total excess entropy of the liquid over the crystal phase; measured heat capacity of the glass and crytal phases; detailed calculation of entropy (S_C, S_E, S_T) and enthalpy of mixing (ΔH_{mix}) parameters for H1 and V1 alloys; additional experimental details, materials, and methods, including methods of *ab initio* molecular dynamics simulations (PDF)

■ AUTHOR INFORMATION

Corresponding Authors

Xiongjun Liu − *Beijing Advanced Innovation Center for Materials Genome Engineering, State Key Laboratory for Advanced Metals and Materials, University of Science and Technology, Beijing, Beijing 100083, China;* orcid.org/0000-0002-1663-4636; Phone: +86-10-6233 2350; Email: xjliu@ustb.edu.cn

Haihui Ruan − *Department of Mechanical Engineering, The Hong Kong Polytechnic University, Kowloon, Hong Kong, China*; Phone: +852-2766 6648; Email: hhruan@polyu.edu.hk

Zhaoping Lu − *Beijing Advanced Innovation Center for Materials Genome Engineering, State Key Laboratory for Advanced Metals and Materials, University of Science and Technology, Beijing, Beijing 100083, China;* orcid.org/0000-0003-1463-8948; Phone: +86-10-8237 5387; Email: luzp@ustb.edu.cn

Authors

Ming Yang − *Beijing Advanced Innovation Center for Materials Genome Engineering, State Key Laboratory for Advanced Metals and Materials, University of Science and Technology, Beijing, Beijing 100083, China; Neutron Science Platform, Songshan Lake Materials Laboratory, Dongguan, Guangdong 523808, China; Institute of Physics, Chinese Academy of Sciences, Beijing 100190, China*

Wenyue Li − *Beijing Advanced Innovation Center for Materials Genome Engineering, State Key Laboratory for Advanced Metals and Materials, University of Science and Technology, Beijing, Beijing 100083, China*

Hui Wang − *Beijing Advanced Innovation Center for Materials Genome Engineering, State Key Laboratory for Advanced Metals and Materials, University of Science and Technology, Beijing, Beijing 100083, China*

Yuan Wu − *Beijing Advanced Innovation Center for Materials Genome Engineering, State Key Laboratory for Advanced Metals and Materials, University of Science and Technology, Beijing, Beijing 100083, China*

Xianzhen Wang − *Institute for Advanced Materials and Technology, University of Science and Technology Beijing, Beijing 100083, China*

Fei Zhang − *Beijing Advanced Innovation Center for Materials Genome Engineering, State Key Laboratory for Advanced Metals and Materials, University of Science and Technology, Beijing, Beijing 100083, China*

Qiaoshi Zeng − *Center for High Pressure Science and Technology Advanced Research, Pudong, Shanghai 201203, China;* orcid.org/0000-0001-5960-1378

Dong Ma − *Neutron Science Platform, Songshan Lake Materials Laboratory, Dongguan, Guangdong 523808, China*

Complete contact information is available at:

https://doi.org/10.1021/acs.jpclett.2c01234
J. Phys. Chem. Lett. 2022, 13, 7889−7897

https://pubs.acs.org/10.1021/acs.jpclett.2c01234

Author Contributions

X.L. and Z.L. initiated the research of the project; W.L. carried out the simulations; Z.L. and X.L. supervised the simulations and analysis. M.Y., X.L., H.R., and Z.L. wrote the paper. M.Y. performed the DSC, low-temperature heat capacity, and Young's modulus measurements and analyzed the data; F.Z. and Q.Z. performed the *in situ* synchrotron experiments. All the authors contributed to the discussion and interpretation of the results.

Notes

The authors declare no competing financial interest.

All data needed to evaluate the conclusions in the paper are present in the paper and/or the Supporting Information. Additional data related to this paper may be requested from the authors.

■ ACKNOWLEDGMENTS

This research was supported by the National Natural Science Foundation of China (Nos. 52071024, 51961160729, 11790293, 51921001, and 51871016). X.L. acknowledges financial support from the Fundamental Research Funds for the Central Universities (No. FRF-GF-20−22B). H.R. gratefully acknowledge the financial support of Hong Kong GRF (No. 15213619). M.Y. acknowledges the Fellowship of China Postdoctoral Science Foundation (No. 2020M680736), the National Natural Science Foundation of China (No. 52101200), and Guangdong Basic and Applied Basic Research Foundation (No. 2020A1515110893). D.M. acknowledges the Guangdong Basic and Applied Basic Research Foundation (No. 2020B1515120077) and the National Natural Science Foundation of China (No. 52130108). The authors thank Mr. Zhibin Li for his help in the preparation of Cover Art.

■ REFERENCES

(1) Angell, C. A. Formation of glasses from liquids and biopolymers. *Science* **1995**, *267* (5206), 1924−1935.
(2) Debenedetti, P. G.; Stillinger, F. H. Supercooled Liquids and the Glass Transition. *Nature* **2001**, *410* (6825), 259−267.
(3) Gibbs, J. H.; Dimarzio, E. A. Nature of the Glass Transition and the Glassy State. *J. Chem. Phys.* **1958**, *28* (3), 373−383.
(4) Adam, G.; Gibbs, J. H. On the Temperature Dependence of Cooperative Relaxation Properties in Glass-Forming Liquids. *J. Chem. Phys.* **1965**, *43* (1), 139−146.
(5) Martinez, L. M.; Angell, C. A. A Thermodynamic Connection to the Fragility of Glass-Forming Liquids. *Nature* **2001**, *410* (6829), 663−667.
(6) Goldstein, M. Viscous Liquids and the Glass Transition: A Potential Energy Barrier Picture. *J. Chem. Phys.* **1969**, *51* (9), 3728−3739.
(7) Fan, Y.; Iwashita, T.; Egami, T. Energy Landscape-driven Non-equilibrium Evolution of Inherent Structure in Disordered Material. *Nat. Commun.* **2017**, *8*, 15417.
(8) Johari, G. P. Contributions to the Entropy of a Glass and Liquid, and the Dielectric Relaxation Time. *J. Chem. Phys.* **2000**, *112* (17), 7518−7523.
(9) Gujrati, P. D.; Goldstein, M. Viscous Liquids and the Glass Transition. 9. Nonconfigurational Contributions to the Excess Entropy of Disordered Phases. *J. Phys. Chem.* **1980**, *84* (8), 859−863.
(10) Sciortino, F.; Kob, W.; Tartaglia, P. Inherent Structure Entropy of Supercooled Liquids. *Phys. Rev. Lett.* **1999**, *83* (16), 3214−3217.
(11) Ozawa, M.; Parisi, G.; Berthier, L. Configurational Entropy of Polydisperse Supercooled Liquids. *J. Chem. Phys.* **2018**, *149* (15), 154501.
(12) Smith, H. L.; Li, C. W.; Hoff, A.; Garrett, G. R.; Kim, D. S.; Yang, F. C.; Lucas, M. S.; Swan-Wood, T.; Lin, J.; Stone, M. B.; et al. Separating the Configurational and Vibrational Entropy Contributions in Metallic Glasses. *Nat. Phys.* **2017**, *13*, 900−906.
(13) Han, D.; Wei, D.; Yang, J.; Li, H. L.; Zaccone, A.; et al. Atomistic Structural Mechanism for the Glass Transition: Entropic Contribution. *Phys. Rev. B* **2020**, *101*, 014113.
(14) Yeh, J. W.; Chen, S. K.; Lin, S. J.; Gan, J. Y.; Chin, T. S.; Shun, T. T.; Tsau, C. H.; Chang, S. Y. Nanostructured High-Entropy Alloys with Multiple Principal Elements: Novel Alloy Design Concepts and Outcomes. *Adv. Eng. Mater.* **2004**, *6* (5), 299−303.
(15) George, E. P.; Raabe, D.; Ritchie, R. O. High-entropy Alloys. *Nat. Rev. Mater.* **2019**, *4* (8), 515−534.
(16) Zhang, Y.; Zuo, T. T.; Tang, Z.; Gao, M. C.; Dahmen, K. A.; Liaw, P. K.; Lu, Z. P. Microstructures and Properties of High-Entropy Alloys. *Prog. Mater. Sci.* **2014**, *61*, 1−93.
(17) Huang, H. L.; Wu, Y.; He, J. Y.; Wang, H.; Liu, X. J.; An, K.; Wu, W.; Lu, Z. P. Phase-transformation Ductilization of Brittle High-entropy Alloys via Metastability Engineering. *Adv. Mater.* **2017**, *29* (30), 1701678.
(18) Li, Z.; Pradeep, K. G.; Deng, Y.; Raabe, D.; Tasan, C. C. Metastable High-entropy Dual-phase Alloys Overcome the Strength−ductility Trade-off. *Nature* **2016**, *534* (7606), 227−230.
(19) Zhao, S. F.; Shao, Y.; Liu, X.; Chen, N.; Ding, H. Y.; Yao, K. F. Pseudo-quinary $Ti_{20}Zr_{20}Hf_{20}Be_{20}(Cu_{20-x}Ni_x)$ High Entropy Bulk Metallic Glasses With Large Glass Forming Ability. *Mater. Des.* **2015**, *87*, 625−631.
(20) Kim, J.; Oh, H. S.; Kim, J.; Ryu, C. W.; Lee, G. W.; Chang, H. J.; Park, E. S. Utilization of High Entropy Alloy Vharacteristics in Er-Gd-Y-Al-Co High Entropy Bulk Metallic Glass. *Acta Mater.* **2018**, *155*, 350−361.
(21) Huo, J. T.; Wang, J. Q.; Wang, W. H. Denary High Entropy Metallic Glass with Large Magnetocaloric Effect. *J. Alloys Compd.* **2019**, *776*, 202−206.
(22) Glasscott, M. W.; Pendergast, A. D.; Goines, S.; Bishop, A. R.; Hoang, A. T.; Renault, C.; Dick, J. E. Electrosynthesis of High-entropy Metallic Glass Nanoparticles for Designer, Multi-functional Electrocatalysis. *Nat. Commun.* **2019**, *10* (1), 2650.
(23) Li, H. F.; Xie, X. H.; Zhao, K.; Wang, Y. B.; Zheng, Y. F.; Wang, W. H.; Qin, L. In Vitro and in Vivo Studies on Biodegradable CaMgZnSrYb High-Entropy Bulk Metallic Glass. *Acta Biomater.* **2013**, *9* (10), 8561−8573.
(24) Yang, M.; Liu, X. J.; Ruan, H. H.; Wu, Y.; Wang, H.; Lu, Z. P. High Thermal Stability and Sluggish Crystallization Kinetics of High-entropy Bulk Metallic Glasses. *J. Appl. Phys.* **2016**, *119* (24), 245112.
(25) Yang, M.; Liu, X. J.; Wu, Y.; Wang, H.; Wang, X. Z.; Lu, Z. P. Unusual Relation Between Glass-forming Ability and Thermal Stability of High-entropy Bulk Metallic Glasses. *Mater. Res. Lett.* **2018**, *6* (9), 495−500.
(26) Jiang, J.; Lu, Z.; Shen, J.; Wada, T.; Kato, H.; Chen, M. W. Decoupling between Calorimetric and Dynamical Glass Transitions in High-entropy Metallic Glasses. *Nat. Commun.* **2021**, *12* (1), 3843.
(27) Allen, M. P.; Tildesley, D. J. *Computer Simulations of Liquids.*; Oxford University: New York, 1987.
(28) Frick, B.; Richter, D. The Microscopic Basis of the Glass Transition in Polymers from Neutron Scattering Studies. *Science* **1995**, *267* (5206), 1939−1945.
(29) Luo, P.; Li, Y. Z.; Bai, H. Y.; Wen, P.; Wang, W. H. Memory effect manifested by a boson peak in metallic glass. *Phys. Rev. Lett.* **2016**, *116* (17), 175901.
(30) Jakse, N.; Nassour, A.; Pasturel, A. Structural and Dynamic Origin of the Boson Peak in a Cu-Zr Metallic Glass. *Phys. Rev. B* **2012**, *85* (17), 174201.
(31) Bünz, J.; Brink, T.; Tsuchiya, K.; Meng, F.; Wilde, G.; Albe, K. Low Temperature Heat Capacity of a Severely Deformed Metallic Glass. *Phys. Rev. Lett.* **2014**, *112* (13), 135501.
(32) Shintani, H.; Tanaka, H. Universal Link between the Boson Peak and Transverse Phonons in Glass. *Nat. Mater.* **2008**, *7*, 870−877.

(33) Angell, C. A.; Yue, Y. Z.; Wang, L. M.; Copley, J. R. D.; Borick, S.; Mossa, S. Potential Energy, Relaxation, Vibrational Dynamics and the Boson Peak, of Hyperquenched Glasses. *J. Phys.Condens. Mater.* **2003**, *15* (11), S1051.
(34) Li, Y.; Bai, H. Y.; Wang, W. H.; Samwer, K. Low-temperature specific-heat anomalies associated with the boson peak in CuZr-based bulk metallic glasses. *Phys. Rev. B* **2006**, *74* (5), 052201.
(35) Widmer-Cooper, A.; Harrowell, P. Free Volume cannot Explain the Spatial Heterogeneity of Debye-Waller Factors in a Glass-forming Binary Alloy. *J. Non-Cryst. Solids* **2006**, *352*, 5098−5102.
(36) Lindemann, F. A. The Calculation of Molecular Vibration Frequencies. *Phys. Z.* **1910**, *11*, 609−611.
(37) Buchenau, U.; Zorn, R.; Ramos, M. A. Probing Cooperative Liquid Dynamics with the Mean Square Displacement. *Phys. Rev. E* **2014**, *90* (4), 042312.
(38) Scher, H.; Zallen, R. Critical Density in Percolation Process. *J. Chem. Phys.* **1970**, *53* (9), 3759−3761.
(39) Grannan, D. M.; Garland, J. C.; Tanner, D. B. Critical Behavior of the Dielectric Constant of a Random Composite near the Percolation Threshold. *Phys. Rev. Lett.* **1981**, *46* (5), 375−378.
(40) Kimura, T.; Tomioka, Y.; Kumai, R.; Okimoto, Y.; Tokura, Y. Diffuse Phase Transition and Phase Separation in Cr-Doped $Nd_{1/2}Ca_{1/2}MnO_3$: A Relaxor Ferromagnet. *Phys. Rev. Lett.* **1999**, *83* (19), 3940−3943.
(41) Phillips, W. A.; Anderson, A. C. *Amorphous Solids: Low-temperature Properties*. Springer-Verlag: Berlin, 1981; Vol. *24*.
(42) Tang, M. B.; Bai, H. Y.; Wang, W. H. Tunneling States and Localized Mode in Binary Bulk Metallic Glass. *Phys. Rev. B* **2005**, *72* (1), 12202.
(43) Li, Y.; Yu, P.; Bai, H. Y. Observation of Low-temperature Specific-heat Anomaly in CuZrAl Bulk Metallic Glasses. *Appl. Phys. Lett.* **2005**, *86* (23), 231909.
(44) Yang, M.; Liu, X. J.; Wu, Y.; Wang, H.; Wang, J. B.; Ruan, H. H.; Lu, Z. P. Elastic Modulus Change and its Relation with Glass-forming Ability and Plasticity in Bulk Metallic Glasses. *Scripta Mater.* **2019**, *161*, 62−65.
(45) Ke, H. B.; Wen, P.; Zhao, D. Q.; Wang, W. H. Correlation between Dynamic Flow and Thermodynamic Glass Transition in Metallic Glasses. *Appl. Phys. Lett.* **2010**, *96* (25), 251902.
(46) Ke, H. B.; Wen, P.; Wang, W. H. The Inquiry of Liquids and Glass Transition by Heat Capacity. *AIP Adv.* **2012**, *2* (4), 041404.
(47) Tang, M.; Wang, W.; Xia, L.; Zhao, J. Constant-Volume Heat Capacity at Glass Transition. *J. Alloys Compd.* **2013**, *577*, 299−302.
(48) Davies, R. O.; Jones, G. O. Thermodynamic and Kinetic Properties of Glasses. *Adv. Phys.* **1953**, *2* (7), 370−410.
(49) Gupta, P. K.; Moynihan, C. T. Prigogine-Defay Ratio for Systems with More than One Order Parameter. *J. Chem. Phys.* **1976**, *65* (10), 4136−4140.
(50) Angell, C. A.; Sichina, W. Thermodynamics of the Glass Transition: Empirical Aspects. *Ann. N.Y. Acad. Sci.* **1976**, *279*, 53−67.
(51) Hempel, E.; Hempel, G.; Hensel, A.; Schick, C.; Donth, E. Characteristic Length of Dynamic Glass Transition near T_g for a Wide Assortment of Glass-Forming Substances. *J. Phys. Chem. B* **2000**, *104* (11), 2460−2466.
(52) Goldstein, M. Viscous Liquids and the Glass Transition. V. Sources of the Excess Specific Heat of the Liquid. *J. Chem. Phys.* **1976**, *64* (11), 4767−4774.
(53) Biroli, G.; Bouchaud, J. P. The Random First-order Transition Theory of Glasses: A Critical Assessment. In *Structural Glasses and Supercooled Liquids: Theory, Experiment, and Applications*; John Wiley & Sons, Inc.: Hoboken, NJ, 2012; p 31−113.
(54) Weiner, J. H. *Statistical Mechanics of Elasticity*; John Wiley & Sons, Inc.: New York, 1983.
(55) Sciortino, F.; Kob, W.; Tartaglia, P. Thermodynamics of Supercooled Liquids in the Inherent-Structure Formalism: a Case Study. *J. Phys.: Condens. Matter* **2000**, *12* (29), 6525−6534.
(56) Heuer, A.; Saksaengwijit, A. Properties of Ideal Gaussian Glass-Forming Systems. *Phys. Rev. E* **2008**, *77* (6), 061507.
(57) Aquino, G.; Allahverdyan, A.; Nieuwenhuizen, T. M. Memory Effects in the Two-Level Model for Glasses. *Phys. Rev. Lett.* **2008**, *101* (1), 015901.
(58) Peyrard, M.; Garden, J. L. Memory Effects in Glasses: Insights into the Thermodynamics of Out-of-equilibrium Systems Revealed by a Simple Model of the Kovacs Effect. *Phys. Rev. E* **2020**, *102* (5), 052122.
(59) Prados, A.; Brey, J. J. The Kovacs effect: a master equation analysis. *J. Stat. Mech-theory E* **2010**, *2010* (02), P02009.
(60) Bertin, E. M.; Bouchaud, J. P.; Drouffe, J. M.; Godreche, C. The Kovacs effect in model glasses. *J. Phys. A: Math. Gen.* **2003**, *36* (43), 10701−10719.
(61) Ruan, H. H.; Zhang, L. C. Modeling of Random Relaxation Paths of Amorphous Material. *J. Am. Ceram. Soc.* **2013**, *96* (6), 1772−1778.
(62) Doliwa, B.; Heuer, A. Energy Barriers and Activated Dynamics in a Supercooled Lennard-Jones liquid. *Phys. Rev. E* **2003**, *67* (3), 031506.
(63) Saksaengwijit, A.; Reinisch, J.; Heuer, A. Origin of the Fragile-to-Strong Crossover in Liquid Silica as Expressed by its Potential-Energy Landscape. *Phys. Rev. Lett.* **2004**, *93* (23), 235701.
(64) Mauro, J. C.; Loucks, R. J. Selenium Glass Transition: A Model Based on the Enthalpy Landscape Approach and Nonequilibrium Statistical Mechanics. *Phys. Rev. B* **2007**, *76* (17), 174202.

https://doi.org/10.1021/acs.jpclett.2c01234
J. Phys. Chem. Lett. 2022, 13, 7889−7897